Inorganic Chemistry

Article

pubs.acs.org/IC

Azadipyrromethene Complexes of d^8 Metal Centers: Rhodium(I), Iridium(I), Palladium(II), and Platinum(II)

Nihal Deligonul and Thomas G. Gray*

Department of Chemistry, Case Western Reserve University, 10900 Euclid Avenue, Cleveland, Ohio 44106, United States

Supporting Information

ABSTRACT: Azadipyrromethenes are blue pigments that chelate main-group and d-block Lewis acids. Reported here are azadipyrromethene complexes of d^8 metal centers. The new compounds are prepared in salt metathesis reactions with chlorinated organometallic precursors. Sixteen new complexes are reported. The principal absorption features are an intense peak near 600 nm and transitions in the ultraviolet; all are characteristic of the azadipyrromethene chromophore. All compounds are dark solids that yield blue or blue-violet solutions. Ten complexes are crystallographically characterized. The structures uniformly show backbone strain, with a *meso*-nitrogen atom that dilates from pure sp^2-hybridization. Structural comparisons are made to related dipyrromethene and tetraazaporphyrin complexes. The electron-donating capacity of azadipyrromethene ligands is evaluated from C≡O stretching frequencies of three rhodium(I) carbonyl complexes and from density-functional theory calculations. Frontier orbitals are confined to the azadipyrromethene ligand. HOMO−LUMO energy gaps are almost unperturbed from those of the free, anionic azadipyrromethene.

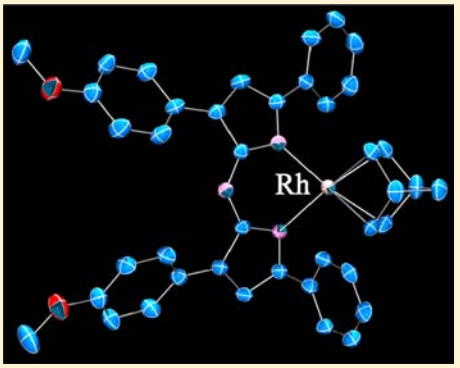

INTRODUCTION

Azadipyrromethenes are conjugated, heterocyclic pigments that have high molar absorptivities near 600 nm and again in the near-ultraviolet.[1] Gram-scale syntheses of azadipyrromethenes only appeared in the past decade,[2−6] and these chromophores have since gained recognition.[7−] The structures of typical azadipyrromethenes, along with the more recent benzannulated analogues,[14,15] appear in Figure 1. In appearance, azadipyrromethene ligands resemble half of a tetra-azaporphyrin or a phthalocyanine. The figure sets out common terminology. Most azadipyrromethenes have the four-aryl anatomy shown in Figure 1, left. The proximal arms are the aryl groups nearer the chelating pocket; those in back are distal. If both proximal arms bear donor atoms, then azadipyrromethenes can become tetradentate ligands.[16−18] Boron adducts of azadipyrromethenes are now numerous, and they have claimed the most attention for sensitization and light-harvesting applications because of their efficient absorption and triplet-state photophysics.

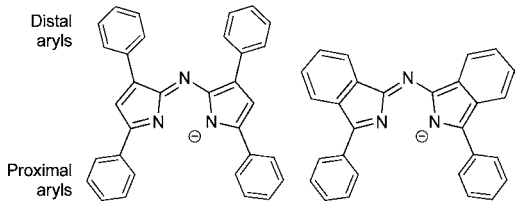

Figure 1. Azadipyrromethene ligands.

The bedrock transition element chemistry of azadipyrromethene ligands continues to develop. Azadipyrromethenes chelate an assortment of other Lewis acids. Bis(azadipyrromethene) complexes of d^{7-9} first-row transition ions and zinc are four-coordinate with compressed tetrahedral stereochemistry.[19−22] Mixed phosphine-azadipyrromethene complexes of copper(I) and silver(I) are trigonal.[23] A mercury(II) bis(azadipyrromethene) complex is four-coordinate in the solid state, with an irregular, distorted tetrahedral structure.[19,24] Gold(I) mono(azadipyrromethene) complexes often have a quasi-linear coordination geometry, or are three-coordinate and trigonal.[25,26] Azadipyrromethenes bind to octahedral metal sites in heteroleptic complexes of rhenium(I).[27] Most such complexes share the absorption features, but usually not the luminescence, of boron azadipyrromethenes. In the solid state, metalla-azadipyrromethenes are frequently crystalline, and often undergo π-stacking.

Square planar rhodium(I), iridium(I), palladium(II), and platinum(II) are archetypal from 16-electron metal centers. For the group 9 ions, π-acceptor complexes predominate. Square complexes are unsaturated, with much enhanced reactivity as a result. For example, the rate constant for exchange of ethylene for 16-electron (acac)Rh$(C_2H_4)_2$ is 10^{14} times greater than from 18-electron (η^5-C_5H_5)Rh$(C_2H_4)_2$ (acac = acetylacetonato).[28] The catalytic literature of these metals fills volumes.[29−41] The related dipyrromethene (dipyrrin) ligands have been much studied in recent years: luminescent compounds, supra-

Received: July 4, 2013
Published: November 6, 2013

   dx.doi.org/10.1021/ic4017239 | *Inorg. Chem.* 2013, 52, 13048−13057

Chart 1. Ligands and Complexes

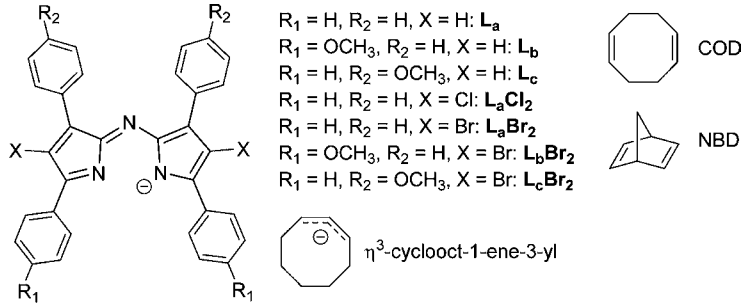

$L_aRh(COD)$	**1**	$L_cRh(CO)_2$	**9**
$L_aIr(COD)$	**2**	$L_cRh(NBD)$	**10**
$L_aRh(CO)_2$	**3**	$L_aPt(\eta^2\text{-}C_2H_4)Cl$	**11**
$L_bRh(COD)$	**4**	$(L_aCl_2)Pt(\eta^2\text{-}C_2H_4)Cl$	**12**
$L_bRh(NBD)$	**5**	$(L_aBr_2)Pt(\eta^2\text{-}C_2H_4)Cl$	**13**
$L_bRh(CO)_2$	**6**	$(L_bBr_2)Pt(\eta^2\text{-}C_2H_4)Cl$	**14**
$L_bIr(COD)$	**7**	$(L_cBr_2)Pt(\eta^2\text{-}C_2H_4)Cl$	**15**
$L_cRh(COD)$	**8**	$L_bPd(\eta^3\text{-cyclooct-1-ene-3-yl})$	**16**

molecular assemblies and their precursors, and catalysts have appeared.[42] Hennessy and Betley[43] have shown the catalytic potential of dipyrrin ligands in direct C−H bond amination reactions mediated by iron complexes of encumbered dipyrromethenes. Considerable interest surrounds the photoactivity of platinum metal complexes, notably for energy conversion and storage.[44−63]

Here we report mononuclear azadipyrromethene complexes of rhodium(I), iridium(I), palladium(II), and platinum(II). Synthetic methods and spectroscopic benchmarks are provided for scientists seeking applications of azadipyrromethenes and related ligands. The new complexes' outstanding feature is a brilliant blue color that originates from the azadipyrromethene. Ligands are of the type shown in Figure 1, left. Syntheses are described, along with optical characterization and crystal structure examples. Density-functional theory (DFT) calculations show highest occupied molecular orbitals (HOMOs) and lowest unoccupied molecular orbitals (LUMOs) centered on the azadipyrromethene; transitions between these orbitals govern the visible absorption profiles. Lower-energy, filled orbitals have admixtures of metal and ligand character.

EXPERIMENTAL SECTION

Manipulations were performed under an atmosphere of purified argon or nitrogen using standard Schlenk and glovebox techniques, and Teflon-coated stir bars. Reagents were commercial in origin and were used without further purification unless indicated. Solvents were HPLC-grade or better, and were dried by passage through activated alumina columns in an MBraun solvent purification system. ^{1}H NMR spectra were collected on a Varian AS-400 spectrometer operating at 399.7 MHz. Chemical shifts (δ) were recorded in parts per million (ppm) relative to tetramethylsilane and referenced to solvent residual peaks. Combustion analyses (C, H, and N) were performed by Robertson Microlit Laboratories. Mass spectrometry was executed at the University of Cincinnati Mass Spectrometry facility. Ultraviolet visible absorption spectra were measured on a Cary 500 spectrophotometer. Infrared spectra were collected in KBr pellets on a Midac Corporation M-series Model M2000. Emission measurements were carried out with a Cary Eclipse spectrophotometer at room temperature; samples were purged with argon for at least 15 min before emission experiments. $[Pd_2(\mu\text{-}Cl)_2(\eta^1,\eta^2\text{-}C_8H_{13})_2]$ was prepared according to a literature procedure.[64] Azadipyrromethenes were synthesized according to O'Shea and co-workers;[4] brominated variants, according to Gao, Deligonul, and Gray.[26]

Chart 1 enumerates compounds.

$L_aRh(COD)$, 1. A 50-mL round-bottom flask was charged with L_a (216 mg, 0.48 mmol), potassium *tert*-butoxide (54 mg, 0.48 mmol), and 5 mL of dry tetrahydrofuran (THF). The resulting bright blue solution was stirred for 30 min. To this solution was added $[(\eta^4\text{-}C_8H_{12})Rh(\mu\text{-}Cl)]_2$ (108 mg, 0.24 mmol) dissolved in THF (3 mL). The reaction mixture was stirred an additional 24 h. The volatiles were removed in vacuo to give a dark red solid, which was washed successively with minimal amounts of acetonitrile and Et_2O. The residue was dissolved in a minimal amount of THF and filtered through Celite in open air. Vapor diffusion of hexanes yielded red, X-ray quality crystals that were analytically pure on drying. Yield: 211 mg (64%). ^{1}H NMR (400 MHz, $CDCl_3$): δ 8.15 (br s, 4H), 8.05 (d, 4H, J = 6.9 Hz), 7.85−7.38 (m, 12H), 7.09 (s, 2H), 3.57 (br s, 2H), 3.30 (br s, 2H), 2.11 (br s, 4H), 1.96 (br s, 4H). UV−vis ($CHCl_3$): λ (ε, M^{-1} cm^{-1}), 303 (47600), 605 (39500), 658 (25000). Anal. Calc. for $C_{40}H_{34}N_3Rh$ (%): C, 72.83; H, 5.20; N, 6.37 Found: C, 72.67; H, 5.19; N, 6.30.

$L_aIr(COD)$, 2. A 50-mL round-bottom flask was charged with L_a (125 mg, 0.28 mmol) and $[(\eta^4\text{-}C_8H_{12})Ir(\mu\text{-}OCH_3)]_2$ (92 mg, 0.14 mmol) and 5 mL of dry THF. The resulting bright blue solution was stirred for 24 h. The volatiles were removed under reduced pressure to give a red solid, which was washed successively with minimal amounts of acetonitrile and Et_2O. The residue was dissolved in THF and filtered through Celite in open air. Vapor diffusion of pentane afforded crimson, X-ray quality crystals. These were analytically pure on drying. Yield: 134 mg (71%). ^{1}H NMR (400 MHz, $CDCl_3$): δ 8.11 (br s, 4H), 8.02 (d, 4H, J = 7.2 Hz), 7.60−7.32 (m, 12H), 7.15 (s, 2H), 3.42 (br s, 2H), 3.17 (br s, 2H), 1.98−1.74 (br s, 4H), 1.39−1.20 (br s, 4H). UV−vis ($CHCl_3$): λ (ε, M^{-1} cm^{-1}), 303 (33100), 401 (6100), 645

dx.doi.org/10.1021/ic4017239 | Inorg. Chem. 2013, 52, 13048−13057

(31200). Anal. Calc. for $C_{40}H_{34}IrN_3$ (%): C, 64.15; H, 4.58; N, 5.61. Found: C, 64.04; H, 4.60; N, 5.54.

$L_aRh(CO)_2$, 3. A 50-mL round-bottom flask was charged with L_a (132 mg, 0.30 mmol), potassium *tert*-butoxide (34 mg, 0.30 mmol), and 5 mL of dry THF. The resulting bright blue solution was stirred for 30 min. $[(CO)_2Rh(\mu\text{-Cl})]_2$ (57 mg, 0.15 mmol) in 3 mL of THF was added by cannula. After stirring for 24 h, the volatiles were removed under reduced pressure, and the residue was washed with acetonitrile and Et_2O. The residue was dissolved in a minimal amount of THF and filtered through Celite in open air. Vapor diffusion of pentane afforded dark ruby-red crystals. Yield: 101 mg (55%). ^{1}H NMR (400 MHz, $CDCl_3$): δ 8.43 (d, 8H, J = 7.3 Hz), 7.63−7.38 (m, 12H), 7.15 (s, 2H). UV−vis ($CHCl_3$): λ (ε, M^{-1} cm^{-1}), 302 (29400), 494 (5990), 633 (32100). IR: ν_{CO}, (cm^{-1}) 2060, 1990. Anal. Calc. for $C_{34}H_{22}N_3O_2Rh$ (%): C, 67.22; H, 3.65; N, 6.92. Found: C, 67.49; H, 3.73; N, 6.81.

$L_bRh(COD)$, 4. A 50-mL round-bottom flask was charged with L_b (72 mg, 0.16 mmol), potassium *tert*-butoxide (18 mg, 0.16 mmol), and 5 mL of dry THF. The resulting dark green solution was stirred for 30 min. To this solution was added $[(\eta^4\text{-}C_8H_{12})Rh(\mu\text{-Cl})]_2$ (38 mg, 0.08 mmol) in 2 mL of THF. After stirring for 24 h, the solvent was removed under reduced pressure, and the residue was washed successively with Et_2O and acetonitrile. The residue was dissolved in a minimal amount of THF and was filtered through Celite in open air. Vapor diffusion of pentane gave X-ray quality dark green crystals. Yield: 82 mg (68%). ^{1}H NMR (400 MHz, $CDCl_3$): δ 8.12 (br s, 2H), 8.04 (d, 4H, J = 7.4 Hz), 7.41−7.32 (m, 8H), 7.13 (d, 4H, J = 8.5 Hz), 7.03 (s, 2H), 3.95 (s, 6H), 3.55 (br s, 2H), 3.40 (br s, 2H), 2.09 (br s, 4H), 1.99 (br s, 4H). UV−vis ($CHCl_3$): λ (ε, M^{-1} cm^{-1}), 323 (23800), 412 (7590), 674 (33100). Anal. Calc. for $C_{42}H_{38}N_3O_2Rh\cdot 1/2\ C_4H_8O$ (%): C, 69.93; H, 5.60; N, 5.56. Found: C, 70.30; H, 5.97; N, 5.44.

$L_bRh(NBD)$, 5. A 50-mL Schlenk flask was charged with L_b (60 mg, 0.11 mmol), potassium *tert*-butoxide (13 mg, 0.11 mmol), and 3 mL of THF. The resulting dark green solution was stirred for 30 min. To this solution was added $[(\eta^4\text{-}C_7H_8)Rh(\mu\text{-Cl})]_2$ (28 mg, 0.06 mmol) in 3 mL of THF. The reaction mixture was stirred for 24 h. Solvent was removed under reduced pressure, and the residue was dissolved in chloroform (2 mL), filtered through Celite in air, and dried under vacuum. The crude product was washed successively with Et_2O and acetonitrile and was then recrystallized twice by vapor diffusion of hexanes into a concentrated solution in THF. Yield: 28 mg (65%). ^{1}H NMR (400 MHz, $CDCl_3$): δ 8.00 (m, 8H), 7.40−7.36 (m, 6H), 7.11 (d, 4H, J = 8.3 Hz), 6.94 (s, 2H), 3.96 (s, 6H), 3.30 (br s, 2H), 3.13 (br s, 4H), 2.17 (br s, 2H). UV−vis ($CHCl_3$): λ (ε, M^{-1} cm^{-1}), 321 (28300), 405 (6850), 490 (9130), 655 (42700). Anal. Calc. for $C_{41}H_{34}N_3O_2Rh$ (%): C, 69.99; H, 4.87; N, 5.97. Found: C, 69.87; H, 4.89; N, 5.98.

$L_bRh(CO)_2$, 6. A 50-mL round-bottom flask was charged with L_b (97 mg, 0.19 mmol), potassium *tert*-butoxide (21 mg, 0.19 mmol), and 5 mL of dry THF and stirred for 30 min. To this mixture was added a solution of $[(CO)_2Rh(\mu\text{-Cl})]_2$ (32 mg, 0.10 mmol) in 3 mL of THF. The reaction mixture was stirred overnight. Solvent was removed under reduced pressure, and the residue was washed successively with Et_2O and acetonitrile. The residue was dissolved in a minimal amount of THF and filtered through Celite in open air. Vapor diffusion of pentane yielded X-ray quality crystals that were analytically pure upon drying. Yield: 38 mg (30%). ^{1}H NMR (400 MHz, $CDCl_3$): δ 8.08 (t, 8H, J = 8.5 Hz), 7.40−7.37 (m, 8H), 7.15 (s, 2H), 7.13 (s, 4H), 3.95 (s, 6H). UV−vis ($CHCl_3$): λ (ε, M^{-1} cm^{-1}), 307 (26400), 410 (6850), 490 (5420), 652 (56200). IR: ν_{CO}, (cm^{-1}) 2057, 1993. Anal. Calc. for $C_{36}H_{28}N_3O_4Rh$ (%): C, 64.58; H, 4.22; N, 6.28. Found: C, 64.71; H, 4.22; N, 6.28.

$L_bIr(COD)$, 7. A 50-mL round-bottom flask was charged with L_b (32 mg, 0.06 mmol), $[(\eta^4\text{-}C_8H_{12})Ir(\mu\text{-}OCH_3)]_2$ (21 mg, 0.03 mmol), and 3 mL of THF. The resulting dark green solution was stirred for 24 h. Solvent was removed under reduced pressure, and the residue was washed successively with acetonitrile and hexanes. The residue was dissolved in a minimal amount of THF, filtered through Celite, and dried under vacuum. Yield: 34 mg (68%). ^{1}H NMR (400 MHz, $CDCl_3$): δ 8.00 (d, 4H, J = 8.5 Hz), 7.90 (d, 4H, J = 7.9 Hz), 7.69 (d, 4H, J = 7.2 Hz), 7.37−7.33 (m, 8H), 7.06 (s, 2H), 3.95 (s, 6H), 3.55 (br s, 2H), 3.46 (br s, 6H), 2.48 (br s, 6H). UV−vis ($CHCl_3$): λ (ε, M^{-1} cm^{-1}), 318 (12500), 414 (4650), 671 (14100). Anal. Calc. for $C_{42}H_{38}IrN_3O_2$ (%): C, 62.36; H, 4.73; N, 5.19. Found: C, 62.01; H, 4.72; N, 5.07.

$L_cRh(COD)$, 8. A 50-mL round-bottom flask was charged with L_b (20 mg, 0.04 mmol), potassium *tert*-butoxide (5 mg, 0.04 mmol), and 5 mL of dry THF. The resulting bright blue solution was stirred for 30 min. To this mixture was added $[(\eta^4\text{-}C_8H_{12})Rh(\mu\text{-Cl})]_2$ (9.7 mg, 0.02 mmol) in 3 mL of THF. The reaction mixture was stirred for 24 h, after which time the solvent was removed under reduced pressure. The crude product was washed successively with Et_2O and acetonitrile. The residue was dissolved in a minimal amount of THF, and was filtered through Celite in open air. The product was then recrystallized twice by vapor diffusion of hexanes into concentrated THF solutions. Yield: 15 mg (50%). ^{1}H NMR (400 MHz, $CDCl_3$): δ 8.15 (br s, 4H), 8.01 (d, 4H, J = 8.9 Hz), 7.51−7.42 (m, 6H), 6.96 (s, 2H), 6.94 (d, 4H, J = 8.98 Hz), 3.89 (s, 6H), 3.56 (br s, 2H), 3.28 (br s, 2H), 2.11 (br s, 4H), 1.96 (br s, 4H). UV−vis ($CHCl_3$): λ (ε, M^{-1} cm^{-1}), 287 (30200), 423 (8010), 659 (35200). Anal. Calc. for $C_{42}H_{38}N_3O_2Rh$ (%): C, 70.09; H, 5.32; N, 5.84. Found: C, 69.93; H, 5.29; N, 5.74.

$L_cRh(CO)_2$, 9. A 50-mL round-bottom flask was charged with L_c (89 mg, 0.18 mmol), potassium *tert*-butoxide (20 mg, 0.18 mmol), and 5 mL of dry THF. The solution was stirred for 30 min. To this solution was added $[(CO)_2Rh(\mu\text{-Cl})]_2$ (34 mg, 0.09 mmol) in 3 mL of THF. The reaction mixture was stirred overnight, after which the solvent was removed under reduced pressure. The crude product was washed successively with Et_2O and acetonitrile. The residue was dissolved in a minimal amount of THF and filtered through Celite in open air. Vapor diffusion of hexanes produced X-ray quality crystals that were analytically pure upon drying. Yield: 70 mg (60%). ^{1}H NMR (400 MHz, $CDCl_3$): δ 8.04 (d, 4H, J = 8.6 Hz), 7.95 (d, 4H, J = 8.9 Hz), 7.62−7.54 (s, 6H), 7.08 (s, 2H), 6.95 (d, 4H, J = 8.9 Hz), 3.89 (s, 6H). IR: ν_{CO}, (cm^{-1}) 2055, 1996. UV−vis ($CHCl_3$): λ (ε, M^{-1} cm^{-1}) 307 (21200), 411 (7670), 491 (5780), 625 (19900), 666 (20400). Anal. Calc. for $C_{36}H_{28}N_3O_4Rh$ (%): C, 64.58; H, 4.22; N, 6.28. Found: C, 64.64; H, 4.24; N, 6.22.

$L_cRh(NBD)$, 10. A 50-mL Schlenk flask was charged with L_c (33 mg, 0.06 mmol), potassium *tert*-butoxide (7 mg, 0.06 mmol), and 5 mL of dry THF. The resulting dark blue solution was stirred for 30 min. To this solution was added $[(\eta^4\text{-}C_7H_8)Rh(\mu\text{-Cl})]_2$ (15 mg, 0.03 mmol) in 3 mL of THF. The reaction mixture was stirred for 24 h, after which time the solvent was removed under reduced pressure. The residue was washed successively with acetonitrile and an ethanol/water mixture (1:1, v/v) to remove unreacted starting materials. The residue was then dissolved in a minimal amount of THF and filtered through Celite in open air. Vapor diffusion of pentane afforded X-ray quality dark ruby crystals. Yield: 12 mg (33%). ^{1}H NMR (400 MHz, $CDCl_3$): δ 7.98−7.95 (m, 6H), 7.57−7.46 (m, 8H), 6.93 (d, 4H, J = 9.8 Hz), 6.87 (s, 2H), 3.87 (s, 6H), 3.73 (br s, 4H), 3.24 (br s, 2H), 3.03 (br s, 2H). UV−vis ($CHCl_3$): λ (ε, M^{-1} cm^{-1}), 300 (17400), 408 (46500), 641 (34400). Anal. Calc. for $C_{41}H_{34}N_3O_2Rh\cdot EtOH\cdot H_2O$ (%): C, 67.27; H, 5.51; N, 5.47. Found: C, 67.45; H, 5.29; N, 5.14.

$L_aPt(\eta^2\text{-}C_2H_4)Cl$, 11. A 50-mL Schlenk flask was charged with L_a (50 mg, 0.11 mmol), potassium *tert*-butoxide (12 mg, 0.11 mmol), and 5 mL of dry THF. The resulting blue solution was stirred for 30 min. A solution of di-μ-chloro-dichlorobis(ethylene)diplatinum(II) (32 mg, 0.06 mmol) in 3 mL of THF was added to the reaction mixture by syringe, and the mixture was stirred for 24 h. The solvent was removed under reduced pressure, and the residue was washed with acetonitrile. The residue was then dissolved in a minimal amount of THF and filtered through Celite in open air. The product was crystallized twice by vapor diffusion of pentane into concentrated THF solutions. Yield: 41 mg (52%). ^{1}H NMR (400 MHz, $CDCl_3$): δ 8.06 (d, 4H, J = 7.3 Hz), 7.96 (d, 4H, J = 7.3 Hz), 7.53 (t, 4H, J = 7.6 Hz), 7.49−7.36 (m, 8H), 7.21 (s, 2H), 4.37 (t, 4H, J = 7.0 Hz). UV−vis ($CHCl_3$): λ (ε, M^{-1} cm^{-1}) 424 (5580), 534 (sh) (8500), 654 (38500). HRMS (ESI): 744.10751. [m/z calc. for $[M+K]^+$: 744.10735]. Anal. Calc for

dx.doi.org/10.1021/ic4017239 | Inorg. Chem. 2013, 52, 13048−13057

$C_{34}H_{26}ClN_3Pt$ (%): C, 54.95; H, 4.07; N, 5.65. Found: C, 55.30; H, 3.69; N, 5.56.

L_aCl_2. To a 100-mL round-bottom flask was added 22.5 mg (50.0 mmol) L_a and 20 mL of chlorobenzene. The mixture was stirred until L_a dissolved. *N*-chlorosuccinimide (20.0 mg, 150 mmol) was added, and the reaction mixture was stirred under argon overnight. Chlorobenzene was removed under reduced pressure, and the crude product washed several times with acetone and then hexanes. The isolated product used without further purification. ^{1}H NMR (400 MHz, CD_2Cl_2): δ 7.41 (d, 4H, J = 7.1 Hz), 7.19 (d, 4H, J = 7.4 Hz), 6.90−6.73 (m, 12H).

(L_aCl_2)Pt(η^2-C_2H_4)Cl, 12. A 50-mL Schlenk flask was charged with L_aCl_2 (97 mg, 0.19 mmol), potassium *tert*-butoxide (21 mg, 0.19 mmol), and 5 mL of dry THF. The resulting turbid dark violet mixture was stirred for 12 h, after which di-μ-chloro-dichlorobis(ethylene)-diplatinum(II) (56 mg, 0.10 mmol) in 3 mL of THF was added by syringe. Stirring continued for 36 h. Solvent was removed under reduced pressure, and the residue was washed successively with water and methanol. The residue was dissolved in a minimal amount of THF and was filtered through Celite. Vapor diffusion of hexanes afforded X-ray quality crystals that were analytically pure upon drying. Yield: 47 mg (32%). ^{1}H NMR (400 MHz, $CDCl_3$): δ 8.12 (t, 3H, J = 5.6 Hz), 7.76 (t, 6H, J = 7.3 Hz), 7.58 (t, 3H, J = 8.1 Hz), 7.38−7.35 (m, 8H), 4.35 (t, 4H, J = 7.0 Hz). UV−vis ($CHCl_3$): λ (ε, M^{-1} cm^{-1}) 372 (6440), 415 (6120), 527 (9150), 663 (28600). Anal. Calc for $C_{34}H_{24}Cl_3N_3Pt{\cdot}CH_3OH$ (%): C, 52.02; H, 3.49; N, 5.20. Found: C, 51.68; H, 3.27; N, 5.17.

(L_aBr_2)Pt(η^2-C_2H_4)Cl, 13. A 50-mL Schlenk flask was charged with L_aBr_2 (80 mg, 0.13 mmol), potassium *tert*-butoxide (14 mg, 0.13 mmol), and 5 mL of dry THF. The resulting turbid dark violet mixture was stirred for 12 h, after which di-μ-chloro-dichlorobis(ethylene)-diplatinum(II) (38 mg, 0.07 mmol) in 3 mL of THF was added by syringe. Stirring continued for 36 h. Solvent was removed under reduced pressure. The resultant dark blue solid was washed successively with ethanol and acetonitrile and dried under reduced pressure. Yield: 47 mg (55%). ^{1}H-NMR (400 MHz, $CDCl_3$): δ 8.09 (d, 2H, J = 5.6 Hz), 7.89 (d, 2H, J = 6.8 Hz), 7.69 (t, 4H, J = 6.8 Hz), 7.64−7.55 (m, 6H), 7.40−7.32 (m, 6H), 4.25 (br s, 4H). UV−vis ($CHCl_3$): λ (ε, M^{-1} cm^{-1}) 427 (5680), 515 (sh) (6440), 657 (28900). Anal. Calc for $C_{34}H_{24}Br_2ClN_3Pt{\cdot}CH_3CH_2OH$ (%): C, 47.46; H, 3.32; N, 4.61. Found: C, 47.46; H, 3.18; N, 4.68.

(L_bBr_2)Pt(η^2-C_2H_4)Cl, 14. A 50-mL Schlenk flask was charged with L_bBr_2 (110 mg, 0.17 mmol), potassium *tert*-butoxide (19 mg, 0.17 mmol), and 5 mL of dry THF. The resulting dark green solution was stirred for 24 h. To this solution was added by syringe di-μ-chloro-dichlorobis(ethylene)diplatinum(II) (50 mg, 0.09 mmol) dissolved in 3 mL of THF. The reaction mixture was stirred for 48 h, after which time the solvent was removed under reduced pressure. The residue was washed successively with ethanol and acetonitrile. The residue was dissolved in a minimal amount of THF and filtered through Celite in open air. Vapor diffusion of hexanes afforded X-ray quality crystals that were analytically pure upon drying. Yield: 89 mg (56%). ^{1}H NMR (400 MHz, $CDCl_3$): δ 8.08 (d, 2H, J = 8.6 Hz), 7.84 (d, 2H, J = 7.9 Hz), 7.67 (t, 4H, J = 6.4 Hz), 7.37−7.30 (m, 6H), 7.07 (d, 4H, J = 8.6 Hz), 4.07 (br s, 4H), 3.96 (s, 3H), 3.92 (s, 3H). UV−vis ($CHCl_3$): λ (ε, M^{-1} cm^{-1}) 439 (13130), 522 (6980), 676 (38400). Anal. Calc for $C_{36}H_{28}Br_2ClN_3O_2Pt$ (%): C, 46.75; H, 3.05; N, 4.54. Found: C, 46.77; H, 3.10; N, 4.47.

(L_cBr_2)Pt(η^2-C_2H_4)Cl, 15. A 50-mL Schlenk flask was charged with L_cBr_2 (107 mg, 0.16 mmol), potassium *tert*-butoxide (18 mg, 0.16 mmol), and 5 mL of dry THF. The resulting suspension was stirred for 24 h. To this mixture was added, by syringe, a solution of di-μ-chloro-dichlorobis(ethylene)diplatinum(II) (47 mg, 0.08 mmol) in 3 mL of THF. After stirring 48 h, the solvent was removed under reduced pressure, and the residue was washed successively with ethanol and acetonitrile. The residue was dissolved in a minimal amount of THF, and the solution was filtered through Celite. Vapor diffusion of pentane yielded a blue product, which was analytically pure upon drying. Yield: 92 mg (63%). ^{1}H NMR (400 MHz, $CDCl_3$): δ 8.08 (d, 2H, J = 7.7 Hz), 7.87 H, J = 7.9 Hz), 7.74−7.70 (m, 4H), 7.62−7.52 (m, 6H), 6.89 (d, 4H, J = 8.9 Hz), 4.06 (br s, 4H), 3.88 (s, 6H). UV−vis ($CHCl_3$): λ (ε, M^{-1} cm^{-1}) 428 (5680), 535 (sh) (8600), 656 (41400). Anal. Calc for $C_{36}H_{28}Br_2ClN_3O_2Pt$ (%): C, 46.75; H, 3.05; N, 4.54. Found: C, 46.81; H, 3.09; N, 4.45.

$L_bPd(\eta^3$-cyclooct-1-ene-3-yl), 16. A 50-mL Schlenk flask was charged with L_b (90 mg, 0.18 mmol), potassium *tert*-butoxide (20 mg, 0.18 mmol), and 5 mL of dry THF. The resulting bright green solution was stirred for 30 min. A solution of $[Pd_2(\mu\text{-}Cl)_2(\eta^1,\eta^2\text{-}C_8H_{13})_2]$ (47 mg, 0.09 mmol) in 3 mL of THF was added by syringe, and the reaction mixture was stirred for 24 h. Solvent was removed under reduced pressure. The residue was washed successively with ethanol and acetonitrile, was dissolved in a minimal amount of THF, and was filtered through Celite in air. Vapor diffusion of pentane afforded X-ray quality crystals. Yield: 31 mg (24%). ^{1}H NMR (400 MHz, $CDCl_3$): δ 8.01 (d, 4H, J = 7.6 Hz), 7.97 (d, 4H, J = 8.4 Hz), 7.39−7.30 (m, 6H), 7.12 (s, 2H), 7.01 (d, 4H, J = 8.5 Hz), 5.04 (t, 1H, J = 8.4 Hz), 3.88 (s, 6H), 3.31 (m, 3H, J = 7.6 Hz), 1.99 (s, 4H), 1.45 (s, 5H). UV−vis ($CHCl_3$): λ (ε, M^{-1} cm^{-1}) 380 (3410), 642 (11500). HRMS (ESI): 723.20715 m/z calc. for $[M+H]^+$: 723.20716.

Crystal Structure Analysis. Single crystal X-ray data were collected on a Bruker AXS SMART APEX CCD diffractometer using monochromatic Mo Kα radiation with the ω scan technique. Unit cells were ascertained using SMART[65] and SAINT+.[66] Data were collected at 100 K (−173 °C). Structures were solved by direct methods; full-matrix least-squares refinement against F^2 with all reflections was performed within SHELXTL.[67] Refinement of extinction coefficients was found to be insignificant. All non-hydrogen atoms were refined anisotropically. All hydrogen atoms were placed in standard calculated positions, and all hydrogen atoms were refined with an isotropic displacement parameter 1.2 times that of the adjacent carbon.

Calculations. Spin-restricted DFT computations proceeded in Gaussian09 rev. A.02.[68] Geometries were optimized without constraint, and harmonic frequency calculations found all real vibrational frequencies, confirming that converged structures are local energy minima. Calculations employed the exchange and correlation functionals of Perdew, Burke, and Ernzerhof,[69] and the TZVP basis set of Godbelt, Andzelm, and co-workers for nonmetals.[70] For metal atoms, the Stuttgart-Dresden effective core potential and basis set were used;[71] scalar relativistic effects are included implicitly. Continuum solvation in chloroform was imposed using the integral equation formalism of the polarizable continuum model.[72−75] Population analyses were performed with the AOMix-CDA program of Gorelsky.[76,77]

RESULTS AND DISCUSSION

Syntheses. Scheme 1 sets out representative syntheses of group 9 and 10 complexes. The neutral azadipyrromethene is mixed with potassium *tert*-butoxide in dry THF to generate the monoanionic ligand in situ. Addition of low-valent precursors affords organometallic complexes in room-temperature salt-metathesis reactions. The products are air-stable, colored solids isolated by precipitation or crystallization. Isolated yields range from 30−71% for Rh(I) and Ir(I) complexes; 24% for Pd(II) complex **16**, and 32−63% for Pt(II) species.

Crystal Structures. Some 10 complexes have been crystallographically authenticated. Attention is limited to geometric parameters involving the metal atom and features that indicate strain in the bound azadipyrromethene. Other ligand-based interatomic distances and angles are normal. Full crystallographic details are available as Supporting Information.

Compounds **1**−**4**, **6**, **9**, and **10** were crystallized by vapor diffusion of pentane or hexanes into THF solutions. The structure of **3** is characteristic. A thermal ellipsoid diagram appears as Figure 2a. Rhodium adopts a square-planar geometry, and the coordination plane is tilted from that of the azadipyrromethene heterocycle. The angle between the

dx.doi.org/10.1021/ic4017239 | Inorg. Chem. 2013, 52, 13048−13057

Scheme 1. Representative Syntheses of Group 9 and 10 Complexes

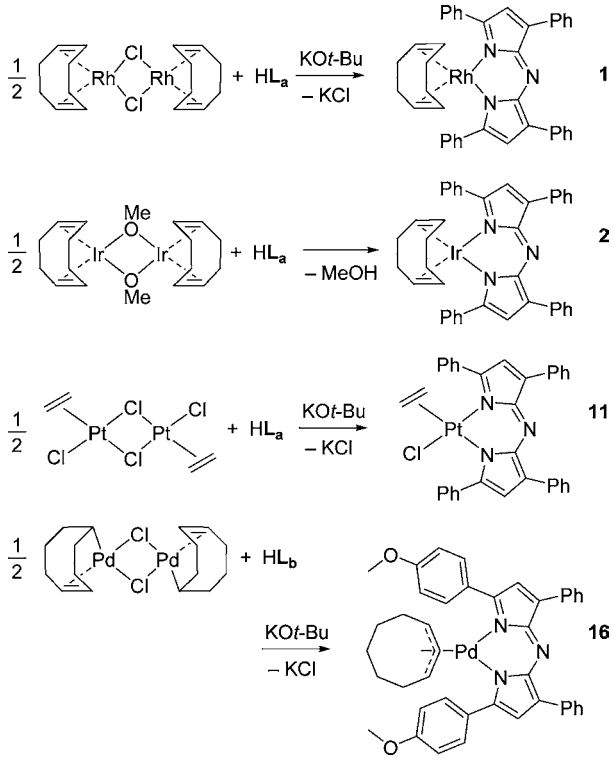

C_{CO}–Rh–C_{CO} plane and the mean plane of the C_8N_3 core is 46.1°. This canting occurs throughout the structures disclosed here and in gold(I),[25,26] rhenium(I),[27] and other mono(azadipyrromethene) complexes[23] of the transition elements. Such canting suggests a strained fit between metals and the azadipyrromethene ligand set. Another indicator of ligand strain is the *meso*-nitrogen atom, which spreads from an idealized geometry for sp^2-hybridization. For **3**, the C–N_{meso}–C angle is 124.4(4)°, and this value is entirely typical. A similar angle (124.0(4)°) is reported for the *meso*-nitrogen atoms of a rhodium(III) octaethyltetraazaporphyrinato (OETAP) complex.[78] Recently Pandey and co-workers[79] have published crystal structures of (COD)Rh^I complexes of dipyrromethene ligands. In these, the backbone C–C_{meso}–C angles are 124.0(5)° and 127.1(5)°. The N3–Rh1–N1 bite angle of **3** is 83.46(17)°. For **1** and **4**, bite angles are 87.92(18)° and 87.94(8)°. The Rh^I azadipyrromethenes herein show more cramped binding clefts than in similar dipyrromethenes. For COD complexes **1** and **4**, backbone C–N_{meso}–C angles are 125.3(3)° and 124.2(3)°; bite angles are 83.51(9)° and 82.19(11)°, respectively. This observation echoes earlier reports[78,80] that OETAP presents a smaller N_4 binding hole than octaethylporphyrin, where the *meso*-carbon atoms are more distended. Neither stacking nor other intermolecular interactions are obvious from the packing diagram.

The central C_8N_3 azadipyrromethene core is not planar but adopts a domed conformation. Figure 2b shows mean planes of the two pentagonal rings; the angle between these planes is 22.5° for **3**. The structure of **6** is notable for having two crystallographically independent complexes in the asymmetric unit. Both show a dome deformation. The angles between mean planes of five-membered rings (within the same complex) are 19.2° and 25.2°. Such a spread in two copies of the same

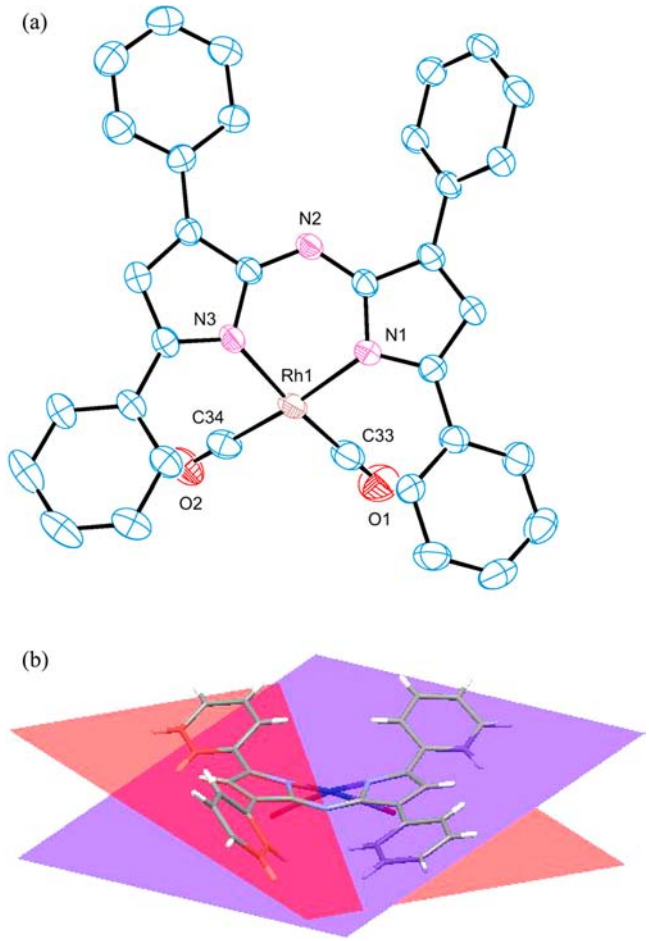

Figure 2. Crystal structure of **3**. (a) Thermal ellipsoids appear at the 50% probability level. Hydrogen atoms are omitted for clarity. A partial atom-labeling scheme is included; unlabeled atoms are carbon. Selected interatomic distances (Å): Rh1–C33, 1.850(7); Rh1–C34 1.868(7); Rh1–N1, 2.058(5); Rh1–N3 2.066(5); C34–O2, 1.137(8); C33–O1, 1.139(7). Selected angles (deg): C33–Rh1–C34; 88.7(3); C33–Rh1–N1, 93.8(2); C34–Rh1–N1, 173.7(2); C33–Rh1–N3, 173.0(2); C34–Rh1–N3, 93.3(2); N1–Rh1–N3, 83.46(17). (b) Mean planes of the pyrrole rings showing ligand doming with an interplanar angle of 22.5°.

complex suggests a malleable backbone with little penalty for bending.

Complexes of group 10 were crystallized by vapor diffusion of pentane or hexanes into THF solutions. Complex **12** exemplifies the platinum(II) complexes encountered here. The structure of **14**, the other crystallographically characterized Pt(II) species complex, is similar. A thermal ellipsoid depiction of **12** appears as Figure 3. Although the platinum–nitrogen bond lengths might have manifested the trans-influences of ethylene and chloride, they are within error of each other (Pt–N trans to C_2H_4: 2.050(4)Å; trans to Cl: 2.047(4) Å). Doming of the azadipyrromethene ligand is evident for **12** (and **14**). For **12**, the angle between mean pyrrin (C_4N) rings is 24.9°.

Compound **16** is the single palladium complex in this study. It is also the only species having a π-allyl-type ligand. The unit cell of **16** contains two crystallographically independent molecules. Figure 4 depicts a thermal ellipsoid rendition of **16**. The hydrocarbon ligand adopts a saddle-shaped conformation and arcs away from the azadipyrromethene; metric parameters are unexceptional. Doming of the azadipyrrome-

dx.doi.org/10.1021/ic4017239 | *Inorg. Chem.* 2013, 52, 13048–13057

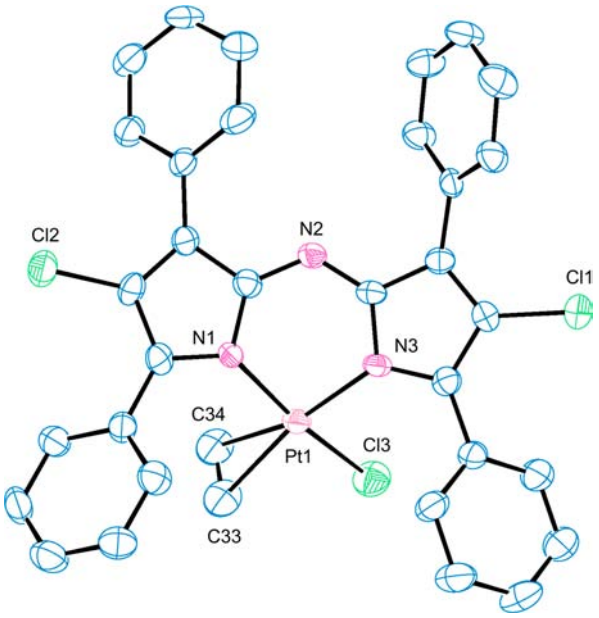

Figure 3. Crystal structure of **12**. Thermal ellipsoids appear at the 50% probability level. Hydrogen atoms are omitted for clarity. A partial atom-labeling scheme is included; unlabeled atoms are carbon. Selected interatomic distances (Å): Pt1−N1, 2.047(4); Pt1−N3, 2.050(4); Pt1−C33, 2.163(6); Pt1−C34, 2.178(6); Pt1−Cl3, 2.3087(17); C33−C34, 1.258(9). Selected angles (deg): N1−Pt1−N3, 85.32(16); N1−Pt1−C33, 99.5(2); N1−Pt1−C34, 90.9(2); N3−Pt1−C34, 159.7(2); C33−Pt1−C34, 33.7(2); N1−Pt1−Cl3, 171.76(12); N3−Pt1−Cl3, 91.42(13); C33−Pt1−Cl3, 85.37(19); C34−Pt1−Cl3, 89.53(19).

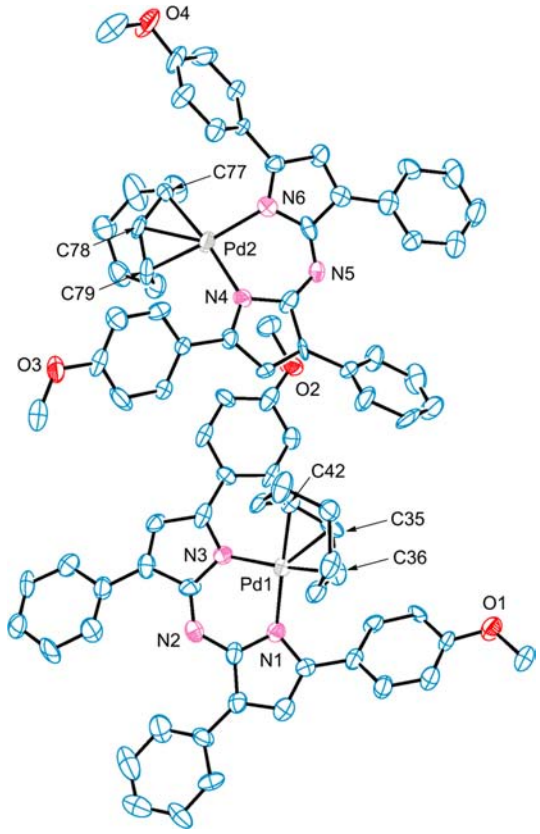

Figure 4. Crystal structure of **16**. The asymmetric unit contains two crystallographically independent molecules. Thermal ellipsoids appear at the 50% probability level. Hydrogen atoms are omitted for clarity. A partial atom-labeling scheme is included; unlabeled atoms are carbon. Selected interatomic distances (Å): Pd1−N1, 2.060(9); Pd1−N3, 2.064(10); Pd1−C35, 2.112(12); Pd1−C42, 2.157(12); Pd1−C36, 2.167(13). Selected angles (deg): N1−Pd1−N3, 86.3(4); N1−Pd1−C35, 136.5(5); N3−Pd1−C35, 137.0(5); N1−Pd1−C42, 167.7(5); N3−Pd1−C42, 101.1(4); C35−Pd1−C42, 38.3(4); N1−Pd1−C36, 101.8(5); N3−Pd1−C36, 164.6(4); C35−Pd1−C36, 38.0(5); C42−Pd1−C36, 68.8(5).

thene is muted compared to that in rhodium(I) complexes. The backbone C−N_{meso}−C angles are 125.4(10)° and 125.5(11)°; these values indicate some angular strain. Structures of **3**, **12**, and **16** have been used to initiate geometry optimizations within DFT, below.

Optical and Infrared Spectroscopy. All new complexes are dark-colored solids that form blue or violet solutions. Figure 5a shows absorption spectra of rhodium and iridium complexes **1**−**10** in chloroform; Figure 5b collects spectra of **11**−**16**. All spectra show a dominant absorption peak near 650 nm, weaker absorptions up to ∼350 nm, and intense features near 300 nm. Spectra are sensitive to methoxy substitution at the 4-position of the proximal phenyl rings, but not in the distal sides. This effect has been described elsewhere.[4,19,23]

Infrared spectra of carbonyl complexes **3**, **6**, and **9** show the expected symmetric and antisymmetric C≡O modes. Table 1 collects frequencies, along with results of a Dapprich−Frenking charge decomposition analysis (below).[81] Also appearing in the table are ν(CO) values of the related carbonyls (acac)Rh(CO)$_2$[82] and CpRh(CO)$_2$.[83] Methoxy substitution of the azadipyrromethene phenyls exerts little effect on the frequency of either mode. Interestingly, the acetylacetonate complex shows higher frequency stretching vibrations than any of **3**, **6**, or **9**, suggesting that acac is the better π-acceptor. (This conjecture holds only if kinematic coupling between the carbonyl stretches and other motions is negligible.) Stretching frequencies of the cyclopentadienyl complex are more similar to those of the azadipyrromethenes, despite the formal six-electron donating character of cyclopentadienide.

Calculations. DFT calculations have been performed to examine the optical and bonding properties of azadipyrromethenes. Complexes **3**, **11**, and **16** are illustrative. Geometry optimizations began from the crystal structures of **3** and **16**, and from that of $\mathbf{L_aCl_2}$ analogue **12**. Converged metrics agree well with crystallographic values, and frequency calculations confirm the optimized geometries to be potential-energy minima. All calculations include a continuum dielectric treatment of chloroform solvation. For all three complexes, the frontier orbitals are relatively isolated in energy.

Figure 6 depicts an energy-level diagram of **3**. The highest-occupied Kohn−Sham orbital (HOMO) is an azadipyrromethene π-function, and likewise the lowest unoccupied Kohn−Sham orbital (LUMO). The HOMO−LUMO energy gap is virtually unchanged from that of free $\mathbf{L_a}^-$. Orbital plots appear at right in the figure. The HOMO − 1 and LUMO + 1, not shown, both have ∼30% Rh character, based on a Mulliken population analysis of the probability density.[84] These correspond, respectively, to the d_{z^2} and $d_{x^2-y^2}$ orbitals of a square planar transition metal center, but both are removed from the frontier energy levels. Calculations on the (unknown) iridium derivative $\mathbf{L_a}$Ir(CO)$_2$ indicate a similar electronic structure, and a partial energy-level diagram appears as Supporting Information, Figure S11.

dx.doi.org/10.1021/ic4017239 | Inorg. Chem. 2013, 52, 13048−13057

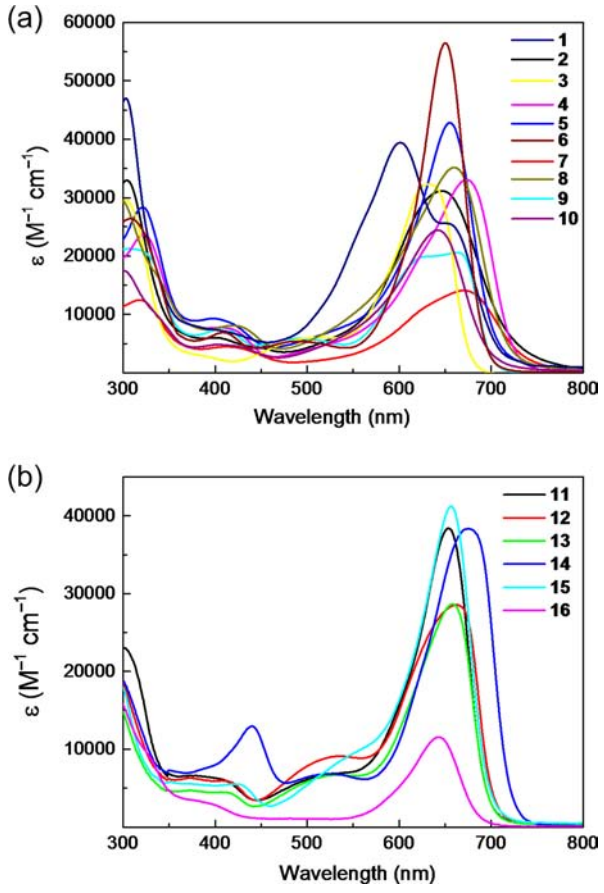

Figure 5. Absorption spectra in chloroform of (a) group 9 and (b) group 10 complexes.

Table 1. Observed Carbonyl Stretching Frequencies in $L_{a-c}Rh(CO)_2$ and Associated Rhodium(I) Complexes; Ligand-to-$Rh(CO)_2^+$ Charge Donation As Calculated by Dapprich–Frenking Charge Decomposition Analysis (CDA)

compound	ν(CO), cm^{-1}	ligand–$Rh(CO)_2$ charge transfer (electrons)
3	2060, 1990	0.72
6	2057, 1993	0.73
9	2055, 1996	0.73
$(acac)Rh(CO)_2$	2070, 2010	0.73
$CpRh(CO)_2$	2050, 1988	1.30

The orbital energy diagram of platinum complex **11**, Figure 7, is broadly like that of rhodium species **3**, Figure 7. The HOMO–LUMO gap is nearly the same as that of L_a^- or **3**. The HOMO and LUMO are isolated from the next orbitals in energy. Both are almost wholly azadipyrromethene-centered.

Figure 8 depicts an energy-level diagram of palladium complex **16**. Here the azadipyrromethene is L_b; that of **3** and **11** is L_a. The HOMO–LUMO gap is again that of the free anion. For methoxy-substituted L_b, this energy is smaller. The HOMO and LUMO, depicted at right in Figure 8, have methoxy contributions. The HOMO–LUMO gap narrows, and the visible absorption profile shifts red. The LUMO + 1 mingles all three fragments: palladium, the hydrocarbyl ligand, and the azadipyrromethene; the HOMO and LUMO are azadipyrromethene π-functions.

Time-dependent DFT (TDDFT) calculations have been performed on the ground-state geometries of **3**, **11**, and **16**.

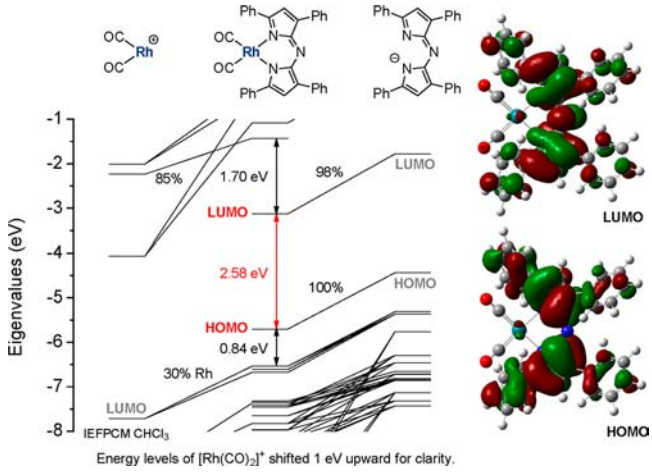

Figure 6. Kohn–Sham orbital energy level diagram of **3**. Compositions of selected orbitals are indicated as percentages of density. Continuum solvation in chloroform is included. Frontier orbital images (contour level 0.02 au) appear at right.

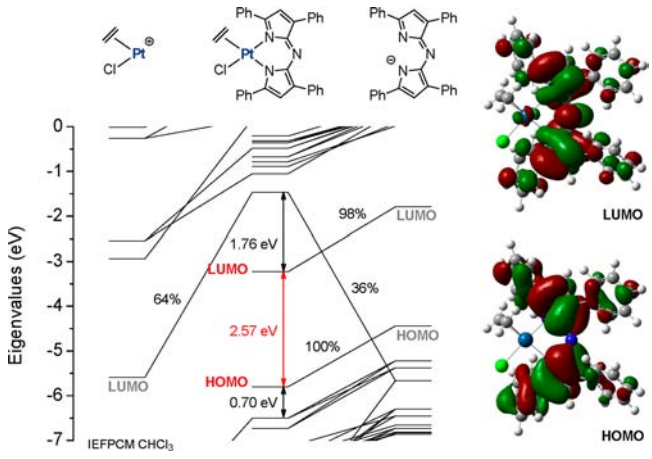

Figure 7. Kohn–Sham orbital energy level diagram of **11**. Compositions of selected orbitals are indicated as percentages of density. Continuum solvation in chloroform is included. Frontier orbital images (contour level 0.02 au) appear at right.

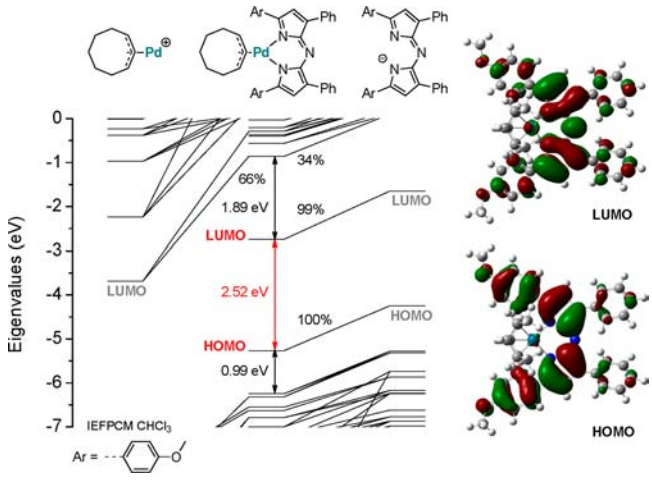

Figure 8. Kohn–Sham orbital energy level diagram of **16**. Compositions of selected orbitals are indicated as percentages of density. Continuum solvation in chloroform is included. Frontier orbital images (contour level 0.02 au) appear at right.

dx.doi.org/10.1021/ic4017239 | *Inorg. Chem.* 2013, 52, 13048–13057

Franck−Condon (FC) singlet excited states have been calculated. For **3**, **11**, and **16**, a clean LUMO←HOMO transition accounts for the intense visible absorption peak near 600 nm. The calculations suggest, therefore, that the common blue color of these complexes arises from an intraligand $\pi-\pi^*$ transition of the azadipyrromethene. There is little or no metal participation.

Dapprich−Frenking charge decomposition analyses have been carried out on carbonyl complexes **3**, **6**, and **9** to compare electron donation from azadipyrromethenes and common related ligands. Results appear in Table 1, alongside measured carbonyl stretching frequencies. The CDA partitioning finds little difference in charge donation among the four-electron donors $\mathbf{L}_{a-c}$ and acac. Net donation from the ligand to $Rh(CO)_2^+$ falls within 0.72−0.73 electrons. Cyclopentadienide is a much stronger electron donor, with net 1.30 electrons transferred to $Rh(CO)_2^+$. These calculations comport with the formal six-electron donating capability of Cp^- compared to formal four-electron donation from acac or azadipyrromethenes.

CONCLUSIONS

Azadipyrromethene complexes of d^8 metal centers form in salt metathesis reactions of the free ligand with potassium *t*-butoxide and organometallic chlorides. The ensuing complexes are stable to air and moisture. Isolated yields range from 24−71%. Crystal structures of 10 complexes indicate bidentate chelation, along with strain in the $C-N_{meso}-C$ hinge. The *meso*-nitrogen distorts from the 120° angle of limiting sp^2 hybridization. The azadipyrromethene kernel is not planar, but domed, having nonparallel pentagonal C_4N rings. The new complexes are all blue or blue-violet chromophores in solution that bear the spectral signatures of BF_2^+-azadipyrromethenes. All share a broad absorption band near 600 nm with molar absorptivities that often exceed 30 000 M^{-1} cm^{-1}.

DFT calculations on rhodium complex **3**, platinum complex **11**, and palladium complex **16** find in each case that the HOMO and LUMO are energetically isolated. These orbitals are π-functions localized on the azadipyrromethene; there is little contribution from the metal or the ancillary ligands. Time-dependent DFT calculations indicate that an allowed LUMO←HOMO transition accounts for their visible absorptions, and hence for their brilliant blue colors. These compounds are entirely representative.

Compounds **3**, **6**, and **9** are rhodium(I) carbonyls that differ only in the azadipyrromethene ligands. Carbonyl stretching frequencies are almost unchanged across the three. The remoteness of the *para*-methoxy substituents ($\mathbf{L}_b$ and $\mathbf{L}_c$) attenuates their electron-releasing effect, as gauged by ν(CO) values, Table 1. CDA calculations suggest that $\mathbf{L}_a-\mathbf{L}_c$ are as Lewis basic as acetylacetonate, another formal four-electron donor. $\mathbf{L}_a-\mathbf{L}_c$ and acac are all considerably less electron-donating than cyclopentadienide, a formal six-electron donor ligand.

This work extends the fundamental coordination chemistry of azadipyrromethene ligands to heavier d^8 metal ions whose primary stereochemistry is square planar. Earlier work shows that azadipyrromethenes tolerate linear, trigonal, flattened tetrahedral, and octahedral metal centers. A mercury(II) bis(azadipyrromethene) complex shows a distorted tetrahedral geometry.[19]

The spectral properties of azadipyrromethenes are narrowly tunable by substitution at carbon[4,23] or by modifying aryl substituents.[11,12] Many times, absorption profiles respond to changes in the bound Lewis acid or its pendant ligands. However, the platinum metals are essentially interchangeable among complexes encountered here. Ligand-centric absorption prevails.

Azadipyrromethenes are finding applications in cellular imaging, photomedicine, and solar energy conversion. Similar ligands support catalysis.[43] The optical and redox properties of azadipyrromethenes and the varied possibilities of their metal complexes offer prospects for enterprising researchers.

ASSOCIATED CONTENT

Supporting Information

X-ray data in .cif format, thermal ellipsoid representations, and tables of crystallographic data; optimized Cartesian coordinates. This material is available free of charge via the Internet at http://pubs.acs.org.

AUTHOR INFORMATION

Corresponding Author

*E-mail: tgray@case.edu. Phone: (216) 368-0991.

Notes

The authors declare no competing financial interest.

ACKNOWLEDGMENTS

This work was supported by the U.S. National Science Foundation, Grant CHE-1057659 to T.G.G. The diffractometer at Case Western Reserve was funded by NSF Grant CHE-0541766. N.D. thanks the Republic of Turkey for a fellowship.

REFERENCES

(1) Abbreviations: acac: acetylacetonate; CDA: charge decomposition analysis, COD: (1*Z*,5*Z*)-cycloocta-1,5-diene; Cp: η^5-cyclopentadienyl; FC: Franck−Condon; HOMO: highest occupied Kohn−Sham orbital; LUMO: lowest unoccupied Kohn−Sham orbital; NBD: bicyclo[2.2.1]hepta-2,5-diene (norbornadiene); OETAP: *meso*-octaethyltetraazaporphyrinato.

(2) Killoran, J.; Allen, L.; Gallagher, J. F.; Gallagher, W. M.; O'Shea, D. F. *Chem. Commun.* **2002**, 1862−1863.

(3) Zhao, W.; Carreira, E. M. *Angew. Chem., Int. Ed.* **2005**, *44*, 1677−1679.

(4) Gorman, A.; Killoran, J.; O'Shea, C.; Kenna, T.; Gallagher, W. M.; O'Shea, D. F. *J. Am. Chem. Soc.* **2004**, *126*, 10619−10631.

(5) McDonnell, S. O.; O'Shea, D. F. *Org. Lett.* **2006**, *8*, 3493−3496.

(6) Hall, M. J.; Allen, L. T.; O'Shea, D. F. *Org. Biomol. Chem.* **2006**, *4*, 776−780.

(7) Gallagher, W. M.; Allen, L. T.; O'Shea, C.; Kenna, T.; Hall, M.; Gorman, A.; Killoran, J.; O'Shea, D. F. *Br. J. Cancer* **2005**, *92*, 1702−1710.

(8) Coskun, A.; Yilmaz, M. D.; Akkaya, E. U. *Org. Lett.* **2007**, *9*, 607−609.

(9) Gao, L.; Senevirathna, W.; Sauvé, G. *Org. Lett.* **2011**, *13*, 5354−5357.

(10) Flavin, K.; Lawrence, K.; Bartelmess, J.; Tasior, M.; Navio, C.; Bittencourt, C.; O'Shea, D. F.; Guldi, D. M.; Giordani, S. *ACS Nano* **2011**, *5*, 1198−1206.

(11) Zhang, X.; Yu, H.; Xiao, Y. *J. Org. Chem.* **2012**, *77*, 669−673.

(12) Gresser, R.; Hartmann, H.; Wrackmeyer, M.; Leo, K.; Riede, M. *Tetrahedron* **2011**, *67*, 7148−7155.

(13) Gao, L.; Tang, S.; Zhu, L.; Sauvé, G. *Macromolecules* **2012**, *45*, 7404−7412.

(14) Gresser, R.; Hummert, M.; Hartmann, H.; Leo, K.; Riede, M. *Chem.—Eur. J.* **2011**, *17*, 2939−2947.

(15) Gresser, R.; Hoyer, A.; Hummert, M.; Hartmann, H.; Leo, K.; Riede, M. *Dalton Trans.* **2011**, *40*, 3476−3483.

(16) Loudet, A.; Bandichhor, R.; Burgess, K.; Palma, A.; McDonnell, S. O.; Hall, M. J.; O'Shea, D. F. *Org. Lett.* **2008**, *10*, 4771−4774.
(17) Nakano, K.; Kobayashi, K.; Nozaki, K. *J. Am. Chem. Soc.* **2011**, *133*, 10720−10723.
(18) Rausaria, S.; Kamadulski, A.; Rath, N. P.; Bryant, L.; Chen, Z.; Salvemini, D.; Neumann, W. L. *J. Am. Chem. Soc.* **2011**, *133*, 4200−4203.
(19) Teets, T. S.; Partyka, D. V.; Updegraff, J. B., III; Gray, T. G. *Inorg. Chem.* **2008**, *47*, 2338−2346.
(20) Palma, A.; Gallagher, J. F.; Müller-Bunz, H.; Wolowska, J.; McInnes, E. J. L.; O'Shea, D. F. *Dalton Trans.* **2009**, 273−279.
(21) Bessette, A.; Ferreira, J. G.; Giguère, M.; Bélanger, F.; Désilets, D.; Hanan, G. S. *Inorg. Chem.* **2012**, *51*, 12132−12141.
(22) Gresser, R.; Hoyer, A.; Hummert, M.; Hartmann, H.; Leo, K.; Riede, M. *Dalton Trans.* **2011**, *40*, 3476−3483.
(23) Teets, T. S.; Updegraff, J. B., III; Esswein, A. J.; Gray, T. G. *Inorg. Chem.* **2009**, *48*, 8134−8144.
(24) Coskun, A.; Yilmaz, M. D.; Akkaya, E. U. *Org. Lett.* **2007**, *9*, 607−609.
(25) Teets, T. S.; Partyka, D. V.; Esswein, A. J.; Updegraff, J. B., III; Zeller, M.; Hunter, A. D.; Gray, T. G. *Inorg. Chem.* **2007**, *46*, 6218−6220.
(26) Gao, L.; Deligonul, N.; Gray, T. G. *Inorg. Chem.* **2012**, *51*, 7682−7688.
(27) Partyka, D. V.; Deligonul, N.; Washington, M. P.; Gray, T. G. *Organometallics* **2009**, *28*, 5837−5840.
(28) Cramer, R. *J. Am. Chem. Soc.* **1972**, *94*, 5681−5685.
(29) *Comprehensive Organometallic Chemistry III*; Crabtree, R. H., Mingos, D. M. P., Eds.; Elsevier: Oxford, U.K., 2007; Vols. 7, 8, 10, and 11, and references therein.
(30) *Modern Rhodium-Catalyzed Organic Reactions*; Evans, P. A., Ed.; Wiley-VCH: Weinheim, Germany, 2005.
(31) *Palladium-Catalyzed Coupling Reactions: Practical Aspects and Future Developments*; Molnár, A., Ed.; Wiley-VCH: Weinheim, Germany, 2013.
(32) *Palladacycles: Synthesis, Characterization, and Applications*; Dupont, J., Pfeffer, M., Eds.; Wiley-VCH: Weinheim, Germany, 2008.
(33) *Metal-Catalyzed Cross-Coupling Reactions*; de Meijere, A., Diederich, F., Eds.; Wiley-VCH: Weinheim, Germany, 2004; Vol. 2.
(34) *Catalyzed Carbon-Heteroatom Bond Formation*; Yudin, A. K., Ed.; Wiley-VCH: Weinheim, Germany, 2011.
(35) *Privileged Chiral Ligands and Catalysts*; Zhou, Q.-L., Ed.; Wiley-VCH: Weinheim, Germany, 2011.
(36) *Iridium Complexes in Organic Synthesis*; Oro, L. A., Claver, C., Eds.; Wiley-VCH: Weinheim, Germany, 2009.
(37) *Iridium Catalysis*; Andersson, P. G., Ed.; Springer: New York, 2011.
(38) van Leeuwen, P. W. N. M.; Chadwick, J. C. *Homogeneous Catalysts: Activity−Stability−Deactivation*; Wiley-VCH: Weinheim, Germany, 2011.
(39) *Innovative Catalysis in Organic Synthesis: Oxidation, Hydrogenation, and C−X Bond Forming Reactions*; Andersson, P. G., Ed.; Wiley-VCH: Weinheim, Germany, 2012.
(40) *The Handbook of Homogeneous Hydrogenation*; de Vries, J. G., Elsevier, C. J., Eds.; Wiley-VCH: Weinheim, Germany, 2007; Vol. 1.
(41) Forum on Palladium Chemistry for Organic Synthesis. *Inorg. Chem.* **2007**, *46*, 1865−1947.
(42) Selected references: (a) Wood, T. E.; Thompson, A. *Chem. Rev.* **2007**, *107*, 1831−1861. (b) Sazanovich, I. V.; Kirmaier, C.; Hindin, E.; Yu, L. H.; Bocian, D. F.; Lindsey, J. S.; Holten, D. *J. Am. Chem. Soc.* **2004**, *126*, 2664−2665. (c) Yu, L.; Muthukumaran, K.; Sazanovich, I. V.; Kirmaier, C.; Hindin, E.; Diers, J. R.; Boyle, P. D.; Bocian, D. F.; Holten, D.; Lindsey, J. S. *Inorg. Chem.* **2003**, *42*, 6629−6647. (d) Cohen, S. M.; Halper, S. R. *Inorg. Chim. Acta* **2002**, *341*, 12−16. (e) Thoi, V. S.; Stork, J. R.; Magde, D.; Cohen, S. M. *Inorg. Chem.* **2006**, *45*, 10688−10697. (f) Do, L.; Halper, S. R.; Cohen, S. M. *Chem. Commun.* **2004**, 2662−2663. (g) McLean, T. M.; Moody, J. L.; Waterland, M. R.; Telfer, S. G. *Inorg. Chem.* **2012**, *51*, 446−455. (h) Scharf, A. B.; Betley, T. A. *Inorg. Chem.* **2011**, *50*, 6837−6845. (i) King, E. R.; Sazama, G. T.; Betley, T. A. *J. Am. Chem. Soc.* **2012**, *134*, 17858−17861. (j) Hanson, K.; Tamayo, A.; Diev, V. V.; Whited, M. T.; Djurovich, P. I.; Thompson, M. E. *Inorg. Chem.* **2010**, *49*, 6077−6084. (k) Filatov, M. A.; Lebedev, A. Y.; Mukhin, S. N.; Vinogradov, S. A.; Cheprakov, A. V. *J. Am. Chem. Soc.* **2010**, *132*, 9552−9554. (l) Bronner, C.; Baudron, S. A.; Hosseini, M. W.; Strassert, C. A.; Guennet, A.; De Cola, L. *Dalton Trans.* **2010**, *39*, 180−184.
(43) Hennessy, E. T.; Betley, T. A. *Science* **2013**, *340*, 591−595.
(44) Gray, H. B.; Maverick, A. W. *Science* **1981**, *214*, 1201−1205.
(45) Lewis, N. S.; Mann, K. R.; Gordon, J. G., II; Gray, H. B. *J. Am. Chem. Soc.* **1976**, *98*, 7461−7463.
(46) Miskowski, V. M.; Sigal, I. S.; Mann, K. R.; Gray, H. B.; Milder, S. J.; Hammond, G. S.; Ryason, P. R. *J. Am. Chem. Soc.* **1979**, *101*, 4383−4385.
(47) Sigal, I. S.; Mann, K. R.; Gray, H. B. *J. Am. Chem. Soc.* **1980**, *102*, 7252−7256.
(48) Rice, S. F.; Miskowski, V. M.; Gray, H. B. *Inorg. Chem.* **1988**, *27*, 4704−4708.
(49) Roundhill, D. M.; Gray, H. B.; Che, C. M. *Acc. Chem. Res.* **1989**, *22*, 55−61 and references therein.
(50) Heyduk, A. F.; Nocera, D. G. *Science* **2001**, *293*, 1639−1641.
(51) Chakraborty, S.; Wadas, T. J.; Hester, H.; Schmehl, R.; Eisenberg, R. *Inorg. Chem.* **2005**, *44*, 6865−6878.
(52) Esswein, A. J.; Veige, A. S.; Nocera, D. G. *J. Am. Chem. Soc.* **2005**, *127*, 16641−16651.
(53) Esswein, A. J.; Nocera, D. G. *Chem. Rev.* **2007**, *107*, 4022−4047.
(54) Sakai, K.; Ozawa, H. *Coord. Chem. Rev.* **2007**, *251*, 2753−2766.
(55) Nocera, D. G. *Inorg. Chem.* **2009**, *48*, 10001−10017.
(56) Teets, T. S.; Cook, T. R.; McCarthy, B. D.; Nocera, D. G. *J. Am. Chem. Soc.* **2011**, *133*, 8114−8117.
(57) Teets, T. S.; Nocera, D. G. *J. Am. Chem. Soc.* **2011**, *133*, 17796−17806.
(58) Teets, T. S.; Cook, T. R.; McCarthy, B. D.; Nocera, D. G. *Inorg. Chem.* **2011**, *50*, 5223−5233.
(59) Lee, C. H.; Cook, T. R.; Nocera, D. G. *Inorg. Chem.* **2011**, *50*, 714−716.
(60) Elgrishi, N.; Teets, T. S.; Chambers, M. B.; Nocera, D. G. *Chem. Commun.* **2012**, *48*, 9474−9476.
(61) Balasubramanian, S.; Wang, P.; Schaller, R. D.; Rajh, T.; Rozhkova, E. A. *Nano Lett.* **2013**, *13*, 3365−3371.
(62) Chakraborty, S.; Wadas, T. J.; Hester, H.; Schmehl, R.; Eisenberg, R. *Inorg. Chem.* **2005**, *44*, 6865−6878.
(63) Powers, D. C.; Chambers, M. B.; Teets, T. S.; Elgrishi, N.; Anderson, L.; Nocera, D. G. *Chem. Sci.* **2013**, *4*, 2880−2885.
(64) Stockland, R. A., Jr.; Anderson, G. K.; Rath, N. P.; Braddock-Wilking, J.; Ellegood, J. C. *Can. J. Chem.* **1996**, *74*, 1990−1997.
(65) *SMART for WNT/2000* , Version 5.628; Bruker AXS Inc.: Madison, WI, 1997−2002.
(66) *SAINT*, Version 6.45; Bruker AXS Inc.: Madison, WI, 1997−2003.
(67) *SHELXTL*, Version 6.10; Bruker AXS Inc.: Madison, WI, 2000.
(68) Frisch, M. J.; Trucks, G. W.; Schlegel, H. B.; Scuseria, G. E.; Robb, M. A.; Cheeseman, J. R.; Scalmani, G.; Barone, V.; Mennucci, B.; Petersson, G. A.; Nakatsuji, H.; Caricato, M.; Li, X.; Hratchian, H. P.; Izmaylov, A. F.; Bloino, J.; Zheng, G.; Sonnenberg, J. L.; Hada, M.; Ehara, M.; Toyota, K.; Fukuda, R.; Hasegawa, J.; Ishida, M.; Nakajima, T.; Honda, Y.; Kitao, O.; Nakai, H.; Vreven, T.; Montgomery, Jr., J. A.; Peralta, J. E.; Ogliaro, F.; Bearpark, M.; Heyd, J. J.; Brothers, E.; Kudin, K. N.; Staroverov, V. N.; Kobayashi, R.; Normand, J.; Raghavachari, K.; Rendell, A.; Burant, J. C.; Iyengar, S. S.; Tomasi, J.; Cossi, M.; Rega, N.; Millam, J. M.; Klene, M.; Knox, J. E.; Cross, J. B.; Bakken, V.; Adamo, C.; Jaramillo, J.; Gomperts, R.; Stratmann, R. E.; Yazyev, O.; Austin, A. J.; Cammi, R.; Pomelli, C.; Ochterski, J. W.; Martin, R. L.; Morokuma, K.; Zakrzewski, V. G.; Voth, G. A.; Salvador, P.; Dannenberg, J. J.; Dapprich, S.; Daniels, A. D.; Farkas, Ö.; Foresman, J. B.; Ortiz, J. V.; Cioslowski, J.; Fox, D. J. *Gaussian 09*, Revision A.02; Gaussian, Inc.: Wallingford, CT, 2009.

(69) Perdew, J. P.; Burke, K.; Ernzerhof, M. *Phys. Rev. Lett.* **1996**, *77*, 3865−3868.
(70) Godbout, N.; Salahub, D. R.; Andzelm, J.; Wimmer, E. *Can. J. Chem.* **1992**, *70*, 560−571.
(71) Dolg, M.; Wedig, U.; Stoll, H.; Preuss, H. *J. Chem. Phys.* **1987**, *86*, 866−872.
(72) Miertus, S.; Scrocco, E.; Tomasi, J. *Chem. Phys.* **1981**, *55*, 117−129.
(73) Tomasi, J.; Mennucci, B.; Cammi, R. *Chem. Rev.* **2005**, *105*, 2999−3093.
(74) Cancès, E.; Mennucci, B.; Tomasi, J. *J. Chem. Phys.* **1997**, *107*, 3032−3041.
(75) Mennucci, B.; Cancès, E.; Tomasi, J. *J. Phys. Chem. B* **1997**, *101*, 10506−10517.
(76) Gorelsky, S. I. *AOMix: Program for Molecular Orbital Analysis*, version 6.81; University of Ottawa, 2013; http://www.sg-chem.net (accessed October 11, 2013).
(77) Gorelsky, S. I.; Lever, A. B. P. *J. Organomet. Chem.* **2001**, *635*, 187−196.
(78) Ni, Y.; Fitzgerald, J. P.; Carroll, P.; Wayland, B. B. *Inorg. Chem.* **1994**, *33*, 2029−2035.
(79) Yadav, M.; Kumar, P.; Pandey, D. S. *Polyhedron* **2010**, *29*, 791−800.
(80) Takenaka, A.; Syal, S. K.; Sasada, Y.; Omura, T.; Ogoshi, T.; Yoshida, Z. *Acta Crystallogr.* **1976**, *B32*, 62−65.
(81) Dapprich, S.; Frenking, G. *J. Phys. Chem.* **1995**, *99*, 9352−9362.
(82) van Eldik, R.; Aygen, S.; Kelm, H.; Trzeciak, A. M.; Ziólkowski, J. J. *Transition Met. Chem.* **1985**, *10*, 167−171.
(83) Smoleński, P. *J. Organomet. Chem.* **2011**, *696*, 3867−3872.
(84) Mulliken, R. S. *J. Chem. Phys.* **1955**, *23*, 1833−1840.